

# STATIC AND DYNAMIC BEHAVIOR OF FLARED-COLUMN BENTS

Suhas S. CHANDANE<sup>1</sup>, David H. SANDERS<sup>2</sup>, M. "Saiid" "SAIDI"<sup>3</sup>, Saad EL-AZAZY<sup>4</sup>

## Abstract

Past earthquakes have shown poor performances of flared-column bents. During the earthquake the plastic hinge was shifted to the base of the flare, increasing the shear demand above the design level and causing shear failure. Caltrans is placing a gap at the top of the flare in order to seismically isolate the flare from the rest of the bent. An experimental and analytical study has been conducted in order to determine the behavior of this system. The project consisted of 4 specimens that were tested on the shake table with two of those specimens being retested statically. In this paper, one of the shake table test will be described that has a gap size that was two times what was used in previous tests. The paper will also describe the two static tests. They were conducted to study the post peak performance of the bents.

## 1. INTRODUCTION

Design of flared columns is complicated due to the varying cross section. In past earthquakes these columns have shown poor performances. Due to the increased capacity of the flared section, the plastic hinge shifted to the bottom of the flare. The columns behaved as if they were much shorter. Therefore, there was an increase in shear demand above the design level causing brittle shear failure. The brittle shear failure can lead to collapse of the structure before achieving sufficient inelastic deformation.

It was assumed in previous designs that flares with small amounts of transverse and longitudinal flare reinforcement would fail during the earthquake and the column core would resist the load. The experimental studies of flared columns show that even lightly reinforced flares contribute to the flexural capacity of the section (Sanchez and Priestley 1997). To solve this problem, Caltrans determined to separate the flares from contributing to the flexural capacity of the column. This was achieved by creating a gap between the flares and the bottom of the beam (Fig. 1). Caltrans came up with these recommendations based on slow-cyclic testing of single columns (Sanchez and Priestley 1997) and not on bents tests. To study the performance of the flares and the behavior of the beam-column connection, shake table tests on the bents were conducted at the University of Nevada Reno (Nada et al. 2002). Three specimens of 1/5 scale were tested, two of them had flexure dominated columns while one had shear dominated columns; this was achieved by using two different column heights. The columns were pinned at the base with two-way hinges. One tall specimen had the transverse flare reinforcement as per current Caltrans recommendations (Caltrans Seismic Design Criteria) (LFCD1) and the other had only minimum transverse reinforcement throughout the flare height (LFCD2). The short specimen had the minimum transverse reinforcement (SFCD2) throughout the flare. The gap at top of the flares was same in all specimens and was as per current specifications.

---

<sup>1</sup>Graduate Research Assistant, Dept. of Civil Engineering, University of Nevada Reno, NV-89557

<sup>2</sup>Associate Professor, Dept. of Civil Engineering, University of Nevada Reno, NV-89557

<sup>3</sup>Professor, Dept. of Civil Engineering, University of Nevada Reno, NV-89557

<sup>4</sup>Senior Design Engineer, California Department of Transportation, Sacramento, CA

The current Caltrans recommendations for flares are as follows:

- Minimum gap thickness 50 mm (2 in) or higher if analysis proved gap closure,
- Nominal longitudinal flare reinforcement, and
- Variable confinement steel ratios.

$$\rho_h = 0.45\% \pm 0.05, \text{ top } 1/3 \text{ of flare}$$

$$\rho_h = 0.075\% \pm 0.025, \text{ bottom } 2/3 \text{ of flare}$$

$$\rho_h = 2 A_b / s D$$

Where,

$\rho_h$  = Confinement steel ratio,

$A_b$  = Area of reinforcement bar,

$s$  = Spacing of the reinforcement, and

$D$  = Diameter of the section.

In the testing of Nada et al., none of the specimens completely failed due to the limits of the shake table. All the specimens showed gap closure at very low ductility and increase in strength after that. In order to fully test the specimens and observe post-peak behavior, it was decided to statically test two of the specimens. The static test on LFCD1 was called LFCD1S and SFCD2 was called SFCD2S. Another issue from the initial series was that the gap at the top of the flare in all specimens closed at a very low level of ductility. Therefore, it was decided to test a short specimen with increased gap width at the top of the flares. The new specimen with increased gap width at the top of the flare was designated as SFCD3.

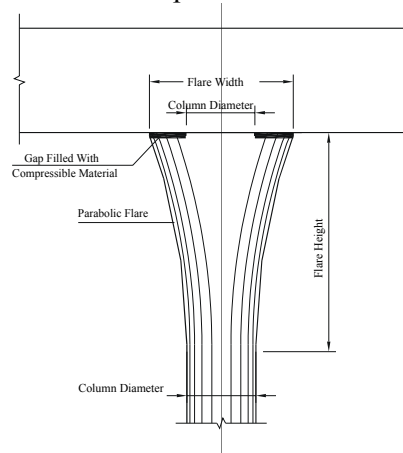


**Figure 1 Layout of the proposed detail**

## 2. PREVIOUS TEST RESULTS

The testing of LFCD1 and SFCD2 was stopped, after significant yielding and gap closure, due to the capacity of the shake table. The specimens did not fail. Figure 2 shows the load-displacement relationships for LFCD1 and SFCD2. Figure shows that the testing was stopped before observing the post-peak load performance of the specimens. Table 1 describes the basic experimental response of the specimens. As the specimens did not fail and their post-peak load performance was not observed, it was decided to test the specimens statically till failure.

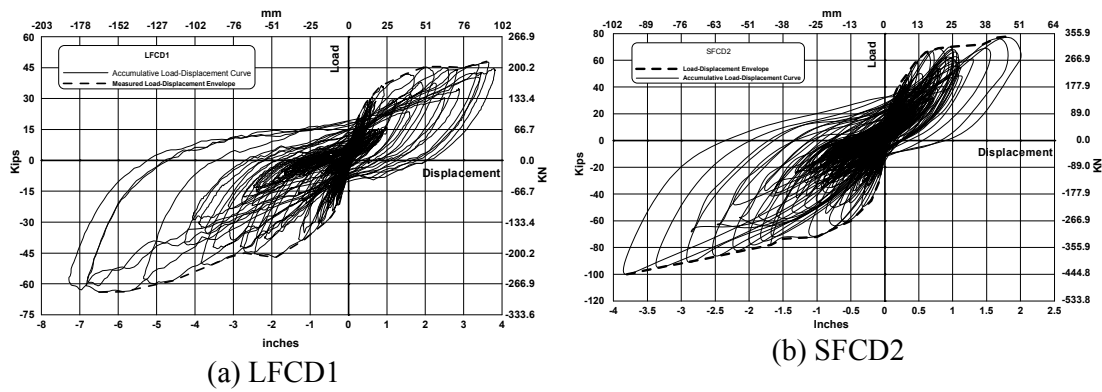


**Figure 2 Load-displacement relationships for LFCD1 and SFCD2**

**Table 1 Structural response of LFCD1 and SFCD2**

	<b>LFCD1</b>	<b>SFCD2</b>
Effective Yield Displacement mm (in)	23.4 (0.92)	10.2 (0.40)
Effective Yield Force KN (Kips)	181.5 (40.8)	279.3 (62.8)
Minimum Displacement mm (in)	165.1 (6.5)	94 (3.7)
Maximum Measured Force KN (Kips)	284.6 (63.98)	433.2 (97.38)
Ductility Ratio	7.07	9.1
Displacement at Gap Closure mm (in)	67.3 (2.65)	42 (1.65)
Ductility Ratio at Gap Closure	2.88	4.0
Ductility Ratio without Base Hinge Disp.	6.12	8.5

### **3. MODEL DESIGN**

Table 2 shows a summary of the characteristics of LFCD1S, SFCD2S and SFCD3. Figure 3 shows the reinforcement details for LFCD1 (LFCD1S). The models were 1/5th scale. The columns of LFCD1 (LFCD1S) were 1625 mm (64 in) tall and in SFCD2 (SFCD2S) and SFCD3 they were 991 mm (39 in). The major change in the new specimen of SFCD3 was the gap at the top of the flare was increased to 19 mm (0.75 in) in comparison to 9.5 mm (0.375 in) in (LFCD1) LFCD1S and SFCD2 (SFCD2S). The 9.5 mm (0.375 in) gap width stands for current Caltrans recommendations. In SFCD3 the confinement steel in the flare was minimum throughout the flare height as it was in LFCD2 and SFCD2 (SFCD2S), while it was as per Caltrans recommendations in LFCD1 (LFCD1S). The beam skin reinforcement in LFCD1 (LFCD1S), LFCD2 and SFCD2 (SFCD2S) had only one reinforcement bar while SFCD3 had distributed skin reinforcement to make it more representative of current specifications. In all specimens the area of the skin reinforcement was the same. Figure 4 shows the reinforcement differences in LFCD1S, SFCD2S and SFCD3. Table 3 gives the material properties for all the specimens.

**Table 2 Flare details for LFCD1S, SFCD2S and SFCD3**

Flare Detail	LFCD1	SFCD2	SFCD3
Transverse reinforcement at top 1/3 of flare height	4.87 mm Dia. @ 28mm (0.192" Dia. @ 1.1")	3.75 mm Dia. @ 97mm (0.148" Dia. @ 3.8")	3.75 mm Dia. @ 97mm (0.148" Dia. @ 3.8")
Transverse Ratio	0.44%	0.08%	0.08%
Transverse reinforcement at remaining 2/3 of flare height	3.75 mm Dia. @ 97mm (0.148" Dia. @ 3.8")	3.75 mm Dia. @ 97mm (0.148" Dia. @ 3.8")	3.75 mm Dia. @ 97mm (0.148" Dia. @ 3.8")
Transverse Ratio	0.08%	0.08%	0.08%
Vertical Flare Reinforcement	6 Wires - 3.75 mm (0.148") Dia.		
Gap width	9.5 mm (0.375")	9.5 mm (0.375")	19 mm (0.75")

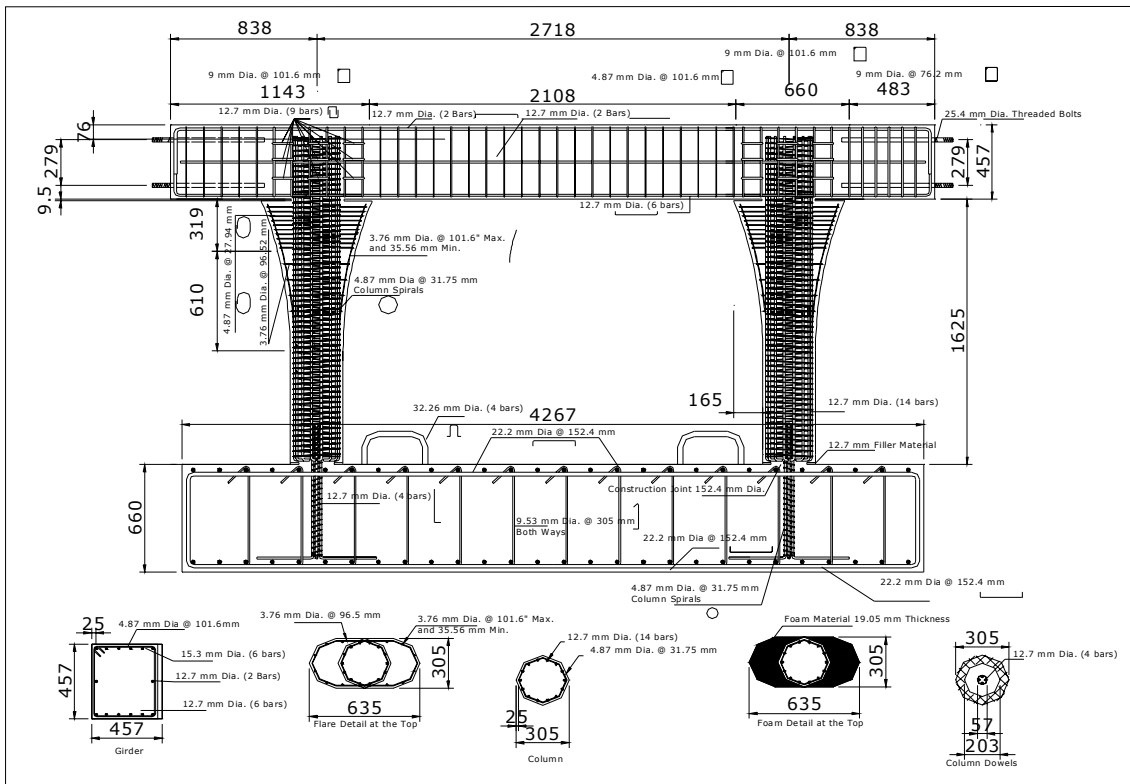


**Figure 3 Reinforcement details for LFCD1S**

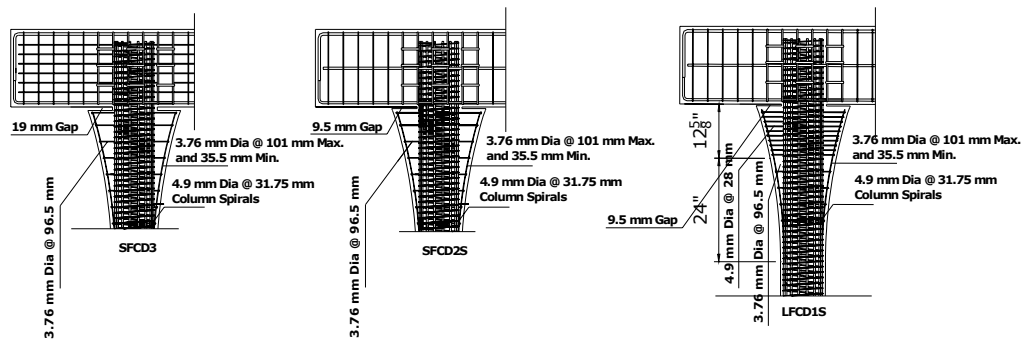


**Figure 4 Reinforcement differences in LFCD1S, SFCD2S and SFCD3**

**Table 3 Material properties for LFCD1S, SFCD2S and SFCD3**

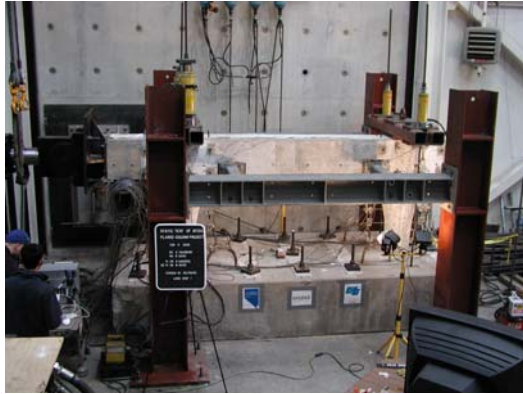
CONCRETE	FOOTING MPa (psi)	COLUMN MPa (psi)	BEAM MPa (psi)
<b>LFCD1S</b>	39(5647)	41(5992)	45(6523)
<b>SFCD2S</b>	42(6089)	45(6549)	43(6278)
<b>SFCD3</b>	41 (5980)	46 (6650)	43 (6180)

STEEL	16 mm (# 5) MPa (ksi)	13 mm (# 4) MPa (ksi)	4.87 mm Bar (0.192 in) MPa (ksi)	3.76 mm Bar (0.148 in) MPa (ksi)
<b>YIELD STRENGTH</b>	483(70)	428(62)	418(60)	492(71)

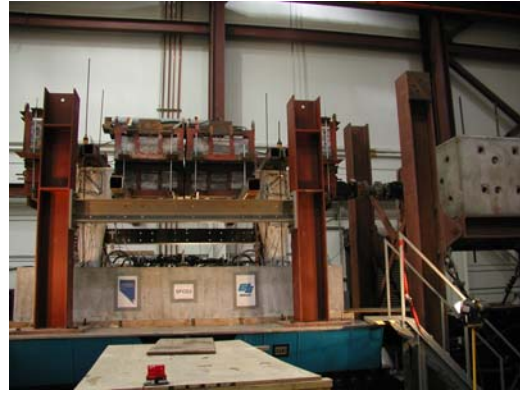
#### **4. TEST SETUPS**

The axial load was set as  $0.1 \times A_g \times f'_c$ ; where  $A_g$  was the gross column cross section area and  $f'_c$  was the concrete compressive strength. The axial load was equal to 400 KN (90 kips) for the system. In the shake table testing the axial load and the inertial loads were created by a combination of lead buckets mounted on the bent as well as hydraulic rams on top of the bent. The capacity of shake table restricted the weight of lead bucket, so some of the axial load was carried by the hydraulic rams. The axial load through the hydraulic rams was self equilibrating and applied directly onto the columns. The strains in the beam longitudinal reinforcement were very low at the beginning of the test indicating a small effect of gravity bending moment in the beam. While the distribution of weight did not exactly model the actual structure, the moments from the gravity load are much smaller than those experienced from the lateral load. The lead weights also apply inertial loads but the hydraulic rams do not, therefore the remaining inertial load equal to the load applied by the hydraulic rams must be applied by an outside source. The remaining inertia loading system is called a mass-rig. It consists of a structure with 4 pins that carries concrete blocks and these blocks are connected to the specimen through a rigid link so that the inertia load is transferred to the specimen. In static testing the total axial loading was applied through hydraulic rams only and an actuator

was used for the lateral load. Figure 5 shows the test setups for the shake table and static tests. The specimens were tied down to the reaction surface with post tensioning bars.



(a) Static test



(b) Shake table test

**Figure 5 Test setups**

For SFCD3 the instrumentation consisted of 154 strain gages, and 57 displacement transducers. Transducers were installed to measure the curvature along the height of the columns, shear displacement in the beam-column connections and the flare, and global displacement of the specimen along with the base-hinge displacement. Accelerometers were used to measure the acceleration of the specimen at different places.

For LFC1S and SFCD2S, 33 displacement transducers were used. They were used to measure the curvature along the column height, shear deformation in the joint, and the global displacement of the specimens including any base slip of the specimen and global movements of the bent.

## **5. LOADING PROGRAM AND PRELIMINARY ANALYSIS**

The loading procedure for the SFCD3 consisted of a series of earthquakes. The runs steps were chosen so that it would capture important points like cracking, yield and ultimate. The specimen was excited with scaled version of the Sylmar record from the 1994 Northridge Earthquake. The accelerations of original records were multiplied by factors. The intensities of earthquakes were 0.25, 0.5, 0.75, 1.0, 1.25, 1.5, 1.75, 2.0, 2.25, 2.5, 2.75, 3.0, 3.25 and 3.5 times Sylmar. This is the same loading program that was used in the study by Nada et al. The peak acceleration for 1.0 times Sylmar was 0.61g.

A preliminary analysis was done using a program called RC-Shake (Laplace 1999) developed at University of Nevada Reno. The program gives the response of the structure to the given earthquake excitation. The program models the specimen as a single degree of freedom system. The program requires a bilinear stiffness curve and mass of the system as well as an acceleration time history. The moment-curvature analysis program RCMC (Wehbe 1997), developed at University of Nevada Reno, was used to calculate effective yield and ultimate points for RC-Shake. Figure 6 shows the response of SFCD3 for intensities of earthquakes from 0.25 to 3.5 times Sylmar.

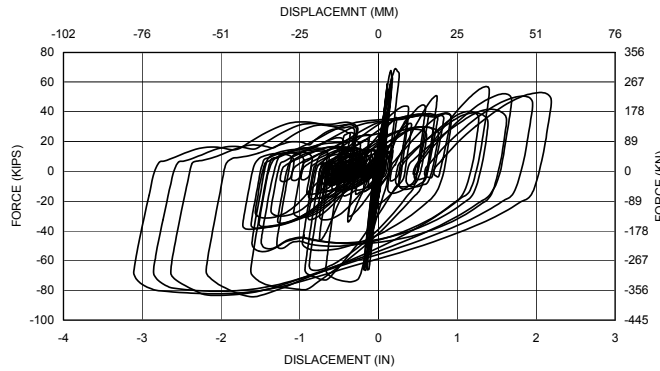


**Figure 6 Load deflection diagram from RC-Shake for Sylmar runs of 0.25, 0.5, 0.75, 1.0, 1.5, 2.0, 2.5, 3.0, 3.25 and 3.5**

LFCD1S and SFCD2S were pushed and pulled through the various points such as first yield, idealized yield, gap closure, and the maximum shake table displacement. The specimens were then pushed and pulled into new displacements until failure. Table 4 shows the loading history for both the specimens. SFCD2S was not pushed to idealized yield displacement. As the first yield displacement and idealized yield displacement were very close to each other, it was decided to push/pull the specimen to the first yield displacement only.

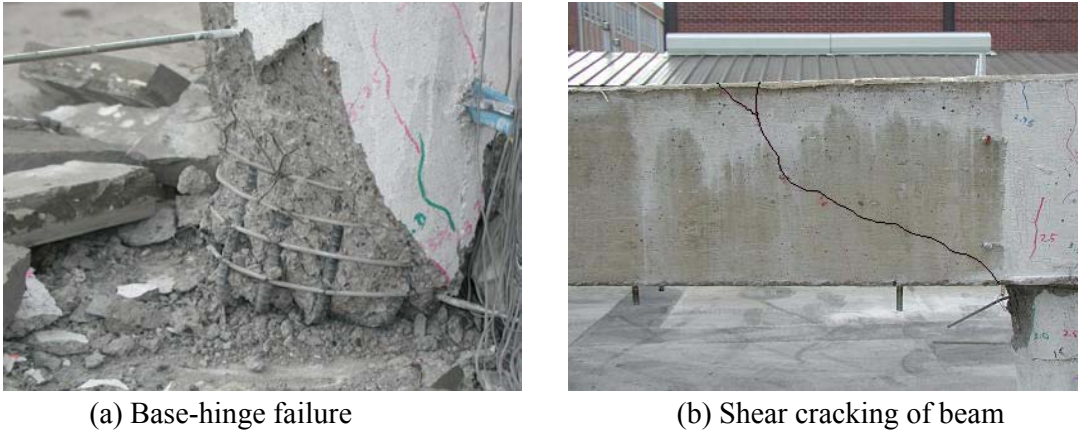
**Table 4 Loading program for LFCD1S and SFCD2S**

<b>PUSH AND PULL</b>	<b>FIRST YIELD</b>	<b>IDEALIZED YIELD</b>	<b>GAP CLOSURE</b>	<b>MAX. SHAKE TABLE DISP.</b>	<b>FINAL PUSH</b>
<b>LFCD1S</b>	17 mm (0.7")	23.4 mm (0.92")	67.3 mm (2.65")	165 mm (6.5")	388 mm (15.3")
<b>SFCD2S</b>	8.4 mm (0.33")	-	41.9 mm (1.65")	94.0 mm (3.70")	134 mm (5.28")

## **6. TEST OBSERVATIONS**

**(1) SFCD3-** The reinforcement in the base-hinge started to yield at 0.5 times Sylmar. The strain data shows that the column longitudinal reinforcement started to yield at 0.75 times Sylmar. Beam bottom longitudinal reinforcement started to yield at 0.75 times Sylmar. Specimen failed in the base-hinge at 3.5 times Sylmar (Figure 7a) with substantial cracking and center spalling at the top of the flare. Figure 8a shows the cumulative load-displacement curve for all runs for SFCD3. The diagram shows the increase in load carrying capacity after significant yielding. This was caused by gap closure. The top of flare came in contact with the beam bottom increasing the effective area of the section; this caused an increase in moment carrying capacity. Significant slippage in the base-hinge was also observed. Shear cracking was observed in the beam after bucket removal (Figure 7b). The increase in moment capacity created an increase in the shear demand in the beam. Table 5 summarizes the response of the structure. Curvature measured along the height of the specimen indicates that plastic hinges were formed at the top and the bottom of the column. Figure 8b compares the load-displacement envelope for SFCD2 and SFCD3. The curve shows gain in strength due to gap closure at higher level of ductility in SFCD3 compared to the SFCD2. The displacement

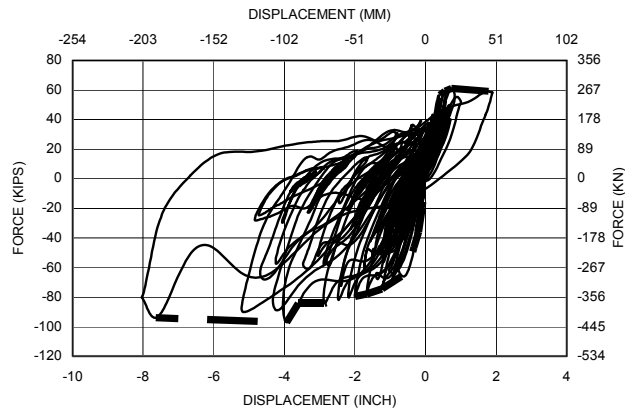
ductility for gap closure in SFCD2 was 4.0, and in SFCD3 it was 6.9. The minimum displacement ductility required by the current specifications is 5. As the gap closure was at a higher level of ductility than required, the gap width of 19 mm (0.75 in) performs well. Figure 9 shows the damaged flare section after the failure with spalling of the flare concrete and damage of the core.



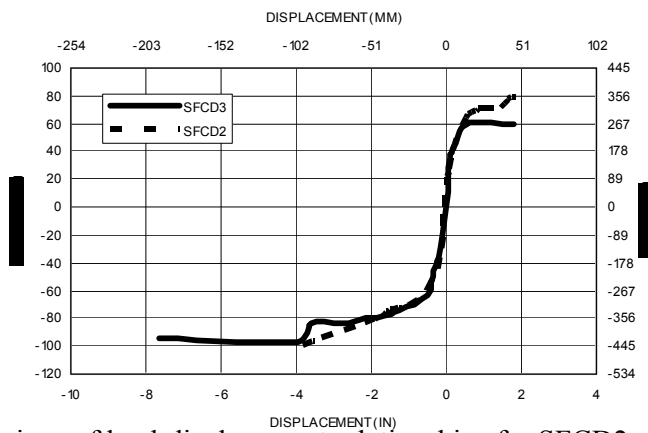
(a) Base-hinge failure

(b) Shear cracking of beam

**Figure 7 SFCD3 at failure**



(a) Load-displacement relationship for SFCD3



(b) Comparison of load-displacement relationships for SFCD2 and SFCD3

**Figure 8 Load-displacement for SFCD2**

**Table 5 Structural response of SFCD3**

	<b>Yield Disp.</b>	<b>Yield Force</b>	<b>Max. Disp.</b>	<b>Max. Force</b>	<b>Drift</b>	<b>Ductility</b>
<b>Ultimate</b>	13.7 mm (0.54 in)	365 KN (82 K)	194 mm (7.64 in)	431 KN (97 K)	16	14.15
<b>Gap Closure</b>	-	-	91.7 mm (3.61 in)	374 KN (84 K)	7.5	6.69



**Figure 9 Damaged flare after the failure of SFCD3**

**(2) LFCD1S-** Wide shear cracks were seen in the beam of LFCD1S but the beam did not fail (Figure 10 a). The test was stopped because of a slight drop in load-carrying capacity and excessive displacements. Figure 11a shows the cumulative load-displacement curve for all loading stages for runs for LFCD1S. Table 6 summarizes the structural response. It shows the maximum ductility of the specimen was 16, this high ductility is due to the fact that the yield point is dominated by the column core section while the final behavior includes the effects of the larger section. Figure 11b compares the load-displacement envelope for LFCD1 and LFCD1S. The LFCD1S is a continuation of LFCD1. Figure 12a shows damaged flare section after the testing.



(a) Large drift and displacement before stopping the testing of LFCD1S

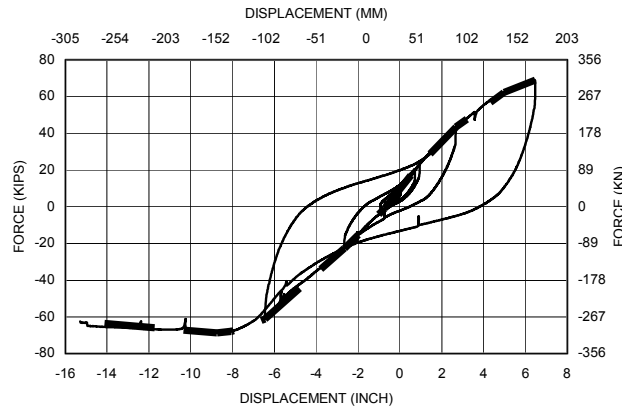


(b) Beam shear failure in SFCD2S

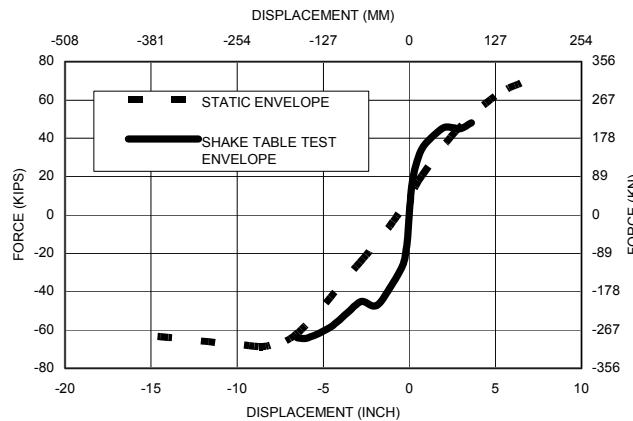
**Figure 10 Behavior of static specimens**

**Table 6 Structural response of LFCD1S and SFCD2S**

	<b>MAX DISP</b>	<b>MAX FORCE</b>	<b>MAX. DRIFT</b>	<b>MAX DUCTILITY</b>
<b>LFCD1S</b>	388 mm (15.3 in)	305 KN (68.6 K)	21 %	16
<b>SFCD2S</b>	134 mm (5.28 in)	482 KN (108.4 K)	11 %	13



(a) Load-displacement relationship for LFCD2S



(b) Comparison of load-displacement relationships for LFCD1 and LFCD2S

**Figure 11 Load-displacement for LFCD1**

(3) **SFCD2S**- Extensive beam shear cracking was seen after gap closure. SFCD2S failed in beam shear (Figure 10b). Figure 13a shows the cumulative load-displacement curve for all loading stages for SFCD2S. Table 6 summarizes the performance of the specimen. The maximum displacement achieved was very high compared to the current specifications. Figure 13b compares the load-displacement envelope for SFCD2 and SFCD2S. The SFCD2S is almost continuing the SFCD2 curve. Figure 12b shows the damaged flare after failure. While the cracking is extensive, the flare is intact.

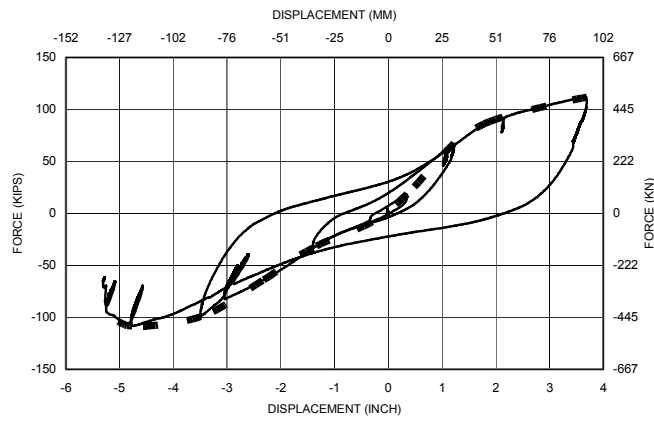


(a) Final condition of LFCD1S after the test

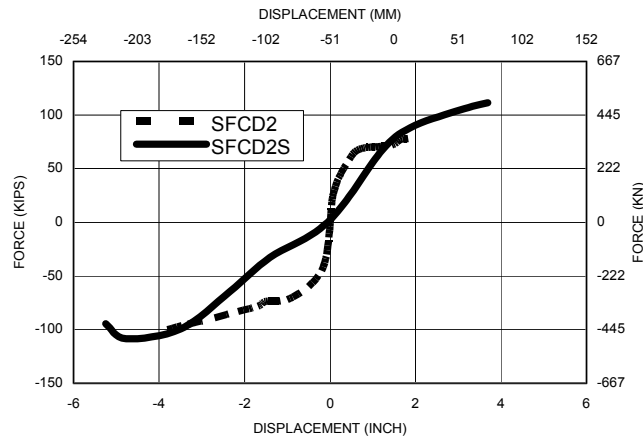


(b) Final condition of SFCD2S

**Figure 12 Final Specimen Condition**



(a) Load-displacement relationship for SFCD2S



(b) Comparison of load-displacement relationships for SFCD2 and SFCD2S

**Figure 13 Load-displacement for SFCD2S**

## 7. GAP WIDTH CALCULATIONS

**(1) Caltrans Method** - Current Caltrans procedure was used to estimate the gap closure status. The procedure is based on curvature analysis of the section. Using the effective yield curvature value and the ultimate curvature value, the yield rotation and plastic rotation at the top section of the flare can be calculated. The yield rotation,  $\theta_y$ , can be calculated using the moment-area method by integrating the moment along the column height. For the plastic rotation,  $\theta_p$ , equation 1 was used.

$$\theta_p = L_p (\phi_u - \phi_y) \quad (1)$$

Where,

$L_p$  = Plastic hinge length,

$\phi_y$  = Effective yield curvature, and

$\phi_u$  = Ultimate yield curvature.

The value of the plastic hinge length is calculated using equation 2 provided by Caltrans.

$$L_p = G + 0.3 f_{ye} d_{bl} \quad (2)$$

Where,

$G$  = Gap width,

$f_{ye}$  = Expected yield stress for longitudinal reinforcement, and

$d_{bl}$  = Bar diameter for longitudinal reinforcement

The total displacement of the flare edge can be calculated by multiplying the total rotation, which is the summation of  $\theta_p$  and  $\theta_y$ , by the distance from the neutral axis of the section at ultimate curvature to the edge of the flare. The gap will not close as long as the calculated deformation is less than the gap width.

For the current specimens, the needed gap width was calculated to be 9.4 mm (0.372 in). The gap width was set at 9.5 mm (0.375 in) for the initial specimens. In the case of SFCD3, the gap was increased to 19 mm (0.75 in) but it still closed. Finite element analysis done by Nada et al. shows that even the specimens with gap width 25 mm (1.0 in) gap closes at a displacement ductility of 10, which is much higher than required.

The procedure was also applied to two flared column specimens statically tested at University of California, San Diego by Sanchez et al: RDS-3 (gap width 25 mm (1.0 in)) and RDS-4 (gap width 50 mm (2.0 in)). The Caltrans Method indicated a require gap size of 18 mm (0.72 in). In RDS-3, the gap width was 25 mm (1.0 in). This specimen showed gap closure at high displacement ductility of 8.2 and drift of 4.7 %, while it failed at a displacement ductility of 13.6 and drift of 7.8 %. In RDS-4, the gap width was 50 mm (2.0 in) and the specimen failed without gap closure. The gap size in which failure in the column will occur at the same time as gap closure is somewhere in between 25 mm (1.0 in) and 50 mm (2.0 in). The Caltrans Method under predicts the needed gap size.

To determine a sufficient gap width to prevent gap closure, a factor of safety is required. The minimum factor of safety of 2 is needed based on the San Diego tests and 3 is needed based on the Reno tests. In order to be conservative, 3 was selected.

**(2) NCHRP 12-49 Method** – NCHRP recommends the minimum gap width of 0.05 times the distance from the center of the column to the extreme edge of the flare or 1.5 times the

calculated plastic hinge rotation from the push-over analysis times the distance from the center of the column to the extreme edge of the flare. NCHRP 12-49 provides an equation for plastic hinge rotation capacity of the section, which can be used to predict the minimum gap width. This minimum gap width is multiplied by 1.5 to determine the required gap width. The equations are 3 through 6.

$$\theta_p = 0.11 (L_p / D') (N_f)^{-0.5} \quad (3)$$

$$N_f = 3.5 (T_n)^{-1/3} \quad (4)$$

$$L_p = L_g + 8800 \varepsilon_y d_b \quad (5)$$

$$L_{G \text{ required}} = \theta_p L_{FLARE} \times 1.5 \quad (6)$$

Where,

$\theta_p$  = Plastic rotation capacity of the section (rad),

$L_p$  = Plastic hinge length,

$D'$  = The distance between the outer layers of the longitudinal reinforcement on opposite faces of the member,

$N_f$  = number of cycles of loading expected at the maximum displacement amplitude,

$T_n$  = natural period of vibration of the structure,

$L_g$  = Gap width provided,

$\varepsilon_y$  = Yield strain of the longitudinal reinforcement,

$d_b$  = Diameter of member longitudinal bar,

$L_{FLARE}$  = Distance from the center of the column to the extreme edge of the flare, and

$L_{G \text{ required}}$  = Minimum gap width required for no gap closure.

For the specimens tested at Reno, 0.05 times the distance from the center of the column to the extreme edge requires a gap size of 16 mm (0.63 in). The plastic rotation procedure gives a minimum gap width of 13 mm (0.52 in) and a required value of 20 mm (0.78 in). As shown from the specimens, this gap would not be sufficient to prevent gap closure.

For the San Diego specimens, the plastic hinge method gives minimum gap width of 22 mm (0.86 in) and a required size of 33 mm (1.29"). The distance from the center to the edge of the flare is 760 mm (30 in.). Therefore, the 0.05 criterion requires a gap size of 38 mm (1.5 in). Therefore, the 0.05 limit is sufficient for the San Diego columns but the plastic hinge method predicts too small of a gap.

Based on a comparison between experimented specimens and the analysis for both the tests at San Diego and Reno, a factor of safety of 2 is needed instead of only 1.5 recommended by the NCHRP method to ensure no gap closure when using the plastic rotation method. An increase in the 0.05 limit is also necessary. Based on the limited test data, a value of 0.08 times the distance from the center of the column to the flare edge should be used.

**(3) Drift Method** - Another way to estimate minimum gap width is with demand drift. Calculating a demand drift and then multiply it with a factor of safety, say 1.5. A required plastic rotation can be calculated from the required demand drift using the equations 7 and 9. This is done assuming that all displacement of the system is handled by the rotation at the top of the column.

$$\Delta_{FDD} = \text{Drift}_{FDD} L_D \quad (7)$$

$$\theta_p = \Delta_{FDD} / H_C \quad (8)$$

$$L_G = \theta_p L_{FLARE} \quad (9)$$

Where,

$\Delta_{FDD}$  = Displacement at factored demand drift,  
Drift<sub>FDD</sub> = Demand drift multiplied by the safety factor,  
 $L_D$  = Height of structure considered for drift,  
 $H_C$  = Height of column,  
 $\theta_P$  = Minimum required plastic hinge rotation for the required demand drift,  
 $L_G$  = Minimum gap width required, and  
 $L_{FLARE}$  = Distance from the center of the column to the extreme edge of the flare.

## **8. CONCLUSIONS**

- (1) All the specimens showed good displacement ductility but current prediction methods do not estimate gap size well
- (2) If there is a chance that the gap will close, shear reinforcement must be added to the beam to handle the additional shear. The reinforcement should be designed based on the analysis of flared column section without gap. In the case of the column shear reinforcement, the size of the flare compensates for the increase in shear demand in the plastic hinge zone. As long as the non-flare portion of the column is not included in any plastic hinge, it should be sufficient.
- (3) Longitudinal beam bottom reinforcement yields very earlier. Increase in its force demand should be considered in design. This is caused by the longitudinal bars not being developed to the top of the beam. This can be predicted by strut-and-tie model (Nada et al.). Hinge bars also yielded very early and further investigation is needed.
- (4) Minimum gap width can be calculated by the Caltrans, NCHRP and Drift method but required a factor of safety.

## **9. ACKNOWLEDGEMENT**

This research was funded by Caltrans. The authors appreciate Caltrans for this support. The authors are also thankful to staff in the laboratory. The opinions expressed in this report are those of authors and do not necessarily represent the opinions of the sponsor.

## **10. REFERENCES**

- (1) Caltrans Seismic Design Criteria, Version 1.1 (July 1999), Caltrans, Sacramento, CA.
- (2) Anthony V. Sanchez, Frieder Seible, and M.J. Nigel Priestley (1997), Seismic Performance of Flared Bridge Columns, Report No. SSRP-97/06, University of California, San Diego.
- (3) Hisham M. Nada, David H. Sanders, and M. "Saiid" Saiidi (2001), Seismic Performance of RC Bridge Frames with Architectural-flared Columns, University of Nevada Reno.
- (4) Nadim I. Wehbe, M. Saiid Saiidi, "User's Manual for RCMC v 1.2", Report No. CCEER-97-4, University of Nevada, Reno.